Scaling of Longitudinally Diode-Pumped Self-Frequency-Doubling Nd : YCOB Lasers

Dennis A. Hammons, Martin Richardson, Bruce H. T. Chai, A. K. Chin, and R. Jollay

***Abstract*—We report the scaling of a new self-frequency-doubling laser, based on the crystal $Nd^{3+}:YCa_4O(BO_3)_3$, to higher powers. The power scaling is achieved by diode pumping using a novel technology of combining the output of up to four high-brightness laser diodes. Spectroscopic, thermo-mechanical, and laser properties are investigated for use in designing high-power self-frequency-doubling lasers. Using a method of angular-multiplexing individual laser diodes for pumping, we demonstrate output powers of more than 1.9 W of fundamental (1060 nm) radiation and 245 mW at the second harmonic. Experimental investigation rendered a thermal stress resistance figure-of-merit for this material to be between 210–280 W/m.**

***Index Terms*—Diode-pumped solid-state laser, nonlinear crystal, self-frequency-doubling.**

I. Introduction

VISIBLE CW laser sources operating efficiently with low cost having a compact design are of immense interest for many applications. Although CW ion lasers are relatively reliable sources operating at several wavelengths, these devices have a low (<1%) electrical–optical conversion and require an undesirable large footprint. The foremost coherent light source in the visible region, the diode laser, can now generate powers of a few tenths of a watt of blue emission to a few watts of red emission [1]. However, its poor spatial quality is inadequate for some applications. Intracavity-doubled solid-state lasers have satisfied many applications by employing a second nonlinear optical medium that converts the infrared-laser radiation to the visible. Recent developments in high-power infrared diodes have brought compact diode-pumped versions of these lasers to the market, with high efficiency and a long life expectancy.

We consider a special case of intracavity doubling (ID) known as self-frequency-doubling (SFD). This method uses a single crystal both as a nonlinear upconversion medium and as a host for lasing ions such as Nd^{3+} or Yb^{3+}. The laser crystal is itself a second-harmonic generator, and, when proper temperature-or angle-tuned phase-matching conditions are met, a portion of the circulating laser power is converted to twice its frequency. Thus, we obtain intracavity frequency doubling without the insertion of a secondary nonlinear-optical medium. Relative to ID using two crystals, an SFD laser has advantages in that it incorporates lower reflection, absorption, and scattering losses and allows a simpler and more robust resonator design. While these are desirable features, unfortunately very few crystals possess the unique combination of optical and physical properties necessary for successful SFD operation.

The recent increase of interest in SFD lasers has been primarily driven by the development of a new family of nonlinear optical crystals, the rare-earth calcium oxyborates ($ReCa_4O(BO_3)_3$) [2]. Advances in this new family of optical materials have primarily been in two particular crystals $YCa_4O(BO_3)_3$ (YCOB) and $GdCa_4O(BO_3)_3$ (GDCOB). Many recent papers have described these materials and their SFD lasing properties when doped with either Nd^{3+} or Yb^{3+} ions [3]–[8]. The first demonstration of SFD laser action was given by Johnson *et al.* [9], with Tm-doped $LiNbO_3$. SFD laser operation using $Nd^{3+}:MgO:LiNbO_3$ [10] was later reported, but was thwarted by poor optical quality and the occurrence of photorefractive damage in the crystal [9]–[11]. A more promising SFD crystal is $Nd^{3+}:YAl_3(BO_3)_4$ (NYAB) due to its large nonlinear coefficients, high emission cross section, and high damage threshold [12], [13]. However, it traditionally suffers from poor optical quality and self-absorption at the second-harmonic wavelength (530 nm) [14]. The recent interest in SFD laser operation has now prompted the investigation of other hosts and the use of Yb^{3+} as a lasing ion [7], [8], [15]–[19].

In this paper, we present spectroscopic and laser properties of $Nd^{3+}:YCOB$ and its potential for scaling as an SFD laser to high powers. In Section II, we present the material characteristics of the $Nd^{3+}:YCOB$ samples used in this report. Section III evaluates the optical properties with a Judd–Ofelt analysis of the polarized absorption spectra and determination of the emission cross section. Section IV describes laser operation of $Nd^{3+}:YCOB$ using a novel high-power diode system as the pump source. Section V gives experimental information on the thermal stress fracture limits, which are necessary in designing high-power laser systems.

II. Material Characteristics of the Experimental Samples

YCOB has many desirable features for a good SFD laser material. This noncentrosymmetric crystal has a BO_3 conjugated ring for both nonlinearity and birefringence. The effective nonlinear coefficient of YCOB for Type I second-harmonic generation (SHG) at 1.06 μm is about 1.1 pm/V [20], comparable to that for LBO, but smaller than most ferroelectric crystals such as KTP and $LiNbO_3$. Although the material is transparent from

Manuscript received November 4, 1999; revised April 25, 2000. This work was supported in part by the State of Florida.

D. A. Hammons is with the Center for Research and Education in Optics and Lasers, University of Central Florida, Orlando, FL 32816-2700 USA.

M. Richardson is with the Center for Research and Education in Optics and Lasers, University of Central Florida, Orlando, FL 32816-2700 USA. He is also with Laser Energetics, Inc., Mercerville, NJ 08619 USA.

B. H. T. Chai is with the Center for Research and Education in Optics and Lasers, University of Central Florida, Orlando, FL 32816-2700 USA. He is also with Crystal Photonics, Inc., Sanford, FL 32773 USA.

A. K. Chin and R. Jollay are with the Polaroid Laser Diode Manufacturing and Development, Norwood, MA 02062 USA.

Publisher Item Identifier S 0018-9197(00)06179-0.

200 to 2600 nm, its birefringence is not large and limits SHG operation to fundamental wavelengths longer than 740 nm and up to 2 μm. In addition, it is nonhydroscopic, so it presents no threat to optical coatings [21]. A measure of the optical damage threshold using a Q-switched Nd : YAG laser at 1064 nm shows it is >1 GW/cm^2, similar to other borate crystals [22]. More importantly for SFD lasers, the YCOB structure has a rare-earth site for active-ion doping by substitution.

All the experimental samples used in the measurements reported here were grown by the Czochralski method from melts contained in iridium crucibles. YCOB crystallizes in the monoclinic biaxial crystal system with the space group Cm [23]. ReCOB compounds have a congruent melting nature; thus, large single crystals with high optical quality can be economically grown [2], [20]. The starting composition melts at 1510 °C and is grown with a rotation rate of 15–20 rpm and is pulled at 1–1.5 mm/h in a neutral atmosphere [20]. Boules, 75 mm in diameter and 200 mm long, are commercially available [2], [20]. The large size also allows for large-aperture nonlinear crystals for high-power lasers. All the samples were either grown at the Crystal Growth Laboratory, CREOL, University of Central Florida, or by Crystal Photonics, Inc.

Some confusion surrounds the description of crystals with low-symmetric, monoclinic systems like YCOB. For crystals with high symmetry such as cubic, tetragonal, etc., both the optical indicatrix axes X, Y, Z and the intrinsic crystallographic axes a, b, c of the crystal are collinear. In the monoclinic system, only the b axis is collinear with the Y axis. The nonorthogonal a and c axes are coplanar but positioned at certain angles with respect to the X and Z axes. The spectroscopic and laser samples have orientations according to Fig. 1. More details regarding the procedure for this orientation can be found in [20].

The 5% doped Nd^{3+} : YCOB laser samples used in this study had a cross section of 3×3 mm and a length of 5 mm. Nd^{3+} : YCOB samples were cut with the X axis collinear with the laser axis. For SFD operation, the crystals were experimentally examined using a Nd : YAG laser to determine the optimum angle for Type I critical phase matching in the XY plane, 90° from the Z axis at 1064 nm. Based on the Sellmeier equations of Iwai *et al.* [21], the crystals were cut at an angle of 33.63° from the X axis. The polished faces had a triple-band anti-reflection coating, which has less than 1% reflectivity at 1060, 530, and 812 nm [24].

Laser crystals for high-power devices need to have high thermal conductivity and high fracture toughness. Fracture toughness is a measure of a material's inherent ability to resist crack propagation and is, therefore, a more suitable gauge of a material's intrinsic strength. ReCOB has weaknesses in both of these aspects. As a nonlinear crystal, the thermal conductivity of YCOB is better than KDP and BBO and is comparable to KTP. However, as a laser medium, the thermal conductivity is about half that of YVO_4 and one-fourth that of YAG. The room-temperature thermal conductivity for each of the crystallographic axes is $\kappa_a = 2.60$ W/mK, $\kappa_b = 2.33$ W/mK, and $\kappa_c = 3.01$ W/mK [6]. The measured thermal-expansion coefficients of YCOB crystals along the crystallographic axes in the range of 20 °C–200 °C are $\alpha_a = 8.39 \times 10^{-6}$°C^{-1}, $\alpha_b = 5.18 \times 10^{-6}$°C^{-1}, and $\alpha_c = 9.17 \times 10^{-6}$°C^{-1} [25].

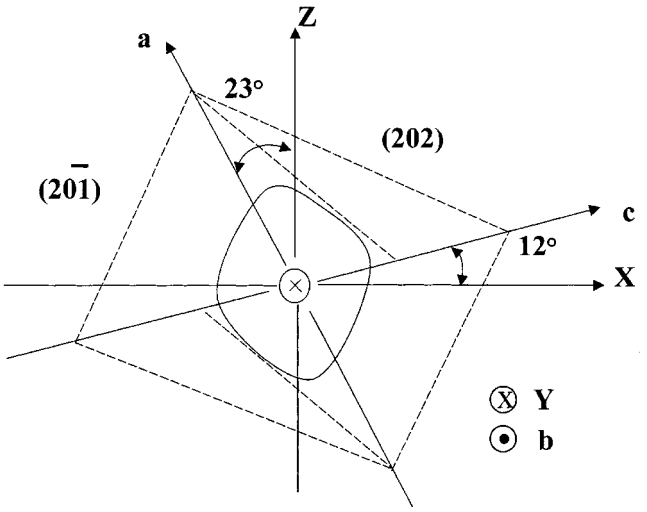

Fig. 1. Orientation of the X, Y, and Z optical indicatrix axes relative to the a, b, and c crystallographic axes of $YCa_4O(BO_3)_3$ [20].

III. Spectroscopy

The polarized optical-absorption spectra from 240 to 1000 nm were measured using a CARY 500 spectrophotometer at room temperature. A Bomem DA8 Fourier-transform spectrometer with high-frequency accuracy (0.004 cm^{-1} at 2000 cm^{-1}) collected the polarized photoluminescence data with a resolution of 16 cm^{-1} with an InGaAs detector operating at 77 K [7]. The photoluminescence excitation was accomplished using an 806-nm laser diode. For all the spectroscopic measurements, the orientation of the samples was such that each optical indicatrix axis was parallel to the pump or probe beam polarization.

Fig. 2 shows the room-temperature polarized absorption spectra along the X, Y, and Z indicatrix axes. The strongest absorption for diode-pumping with AlGaAs laser diodes occurs for light polarized along the Z axis with the two peaks at 794 nm and 812 nm. The optical behavior of Nd^{3+} ions in this low site symmetry varies as the optical propagation direction is rotated from the X axis to the Y axis [26]. The absorption coefficient varies with angle and has been measured to be 2.9 cm^{-1} at 28° and 3.8 cm^{-1} at 35° from the X axis for SFD laser operation in the red at 666 nm and in the green at 530 nm [4], [6]. We also see that the absorption coefficient for the second harmonic of 1060 nm in the polarization perpendicular to the lasing polarization is 0.46 cm^{-1}. For approximately the same doping percentage, this is approximately half the absorption coefficient for NYAB at 531 nm of 0.94 cm^{-1} [12].

The evaluation and prediction of the transition probabilities of the Nd^{3+} ion have been well described for determining the emission cross sections [27]–[31]. In a similar analysis, we begin by determining the line strength S_{meas} of the transition between the ground $^4I_{9/2}$ manifold and the excited J manifolds using [27]

$$S_{\text{meas}} = \frac{3ch(2J+1)}{8\pi^3 e^2 \overline{\lambda}} \cdot \frac{9n}{(n^2+2)^2} \int \sigma_{\text{abs}}(\lambda)\, d\lambda \quad (1)$$

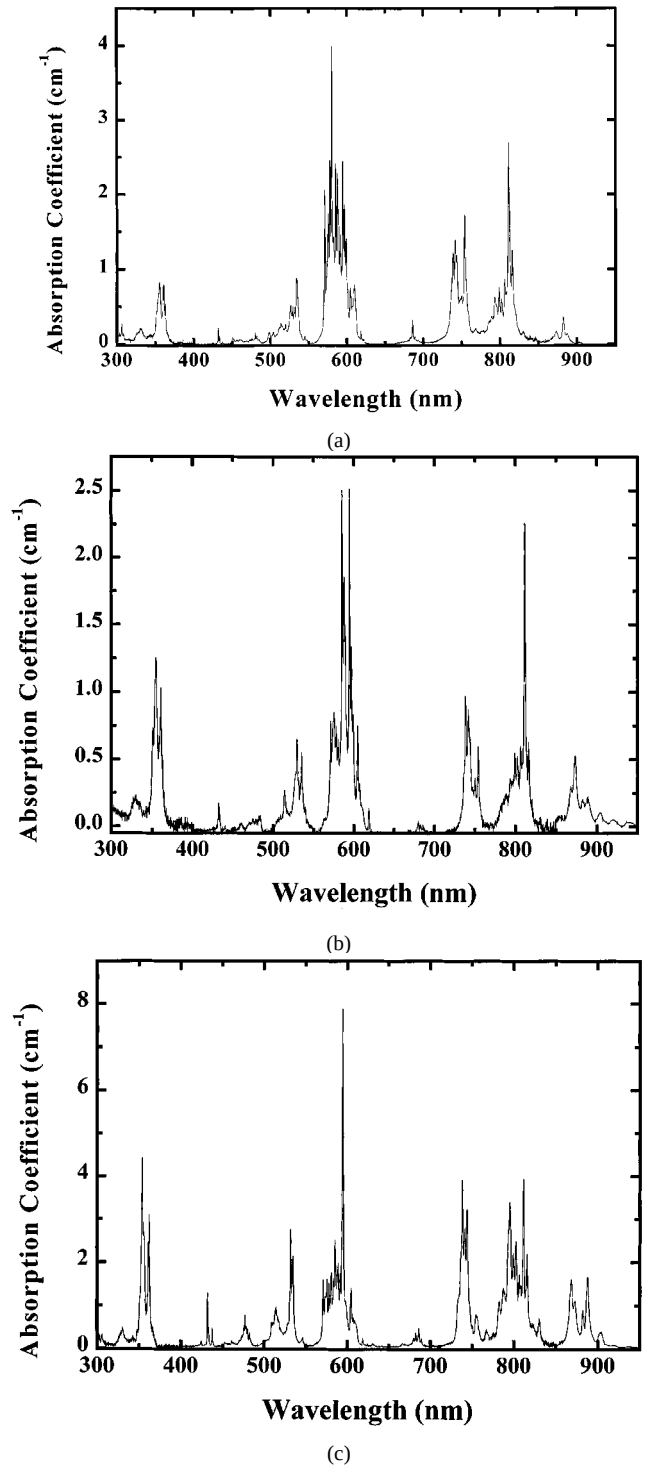

Fig. 2. Polarized absorption spectra of 5% doped $Nd^{3+}:YCa_4O(BO_3)_3$ for light polarized along the (a) X, (b) Y, and (c) Z optical indicatrix axes

where $\sigma_{\rm abs}(\lambda)$ is the absorption cross section at wavelength λ, $\overline{\lambda}$ is the mean wavelength of the band, J is the total angular momentum quantum number of the initial level (for Nd^{3+} $J = 9/2$), c is the speed of light in vacuum, h is Planck's constant, e is the electron energy, and $n = n(\overline{\lambda})$ for the index of refraction at wavelength $\overline{\lambda}$. The analysis of the absorption spectra is performed with line strength measurements made using light polarized parallel to the indicated indicatrix axis. Average line strengths are then calculated by averaging the parallel values with equal weight [31]. Calculation of the absorption cross section is obtained using an ion concentration of 4.7 at.%, which gives an Nd concentration of $\sim 2.1 \times 10^{20}$ ions/cm^3 [20]. The peak absorption cross section for the ${}^4F_{3/2} \rightarrow {}^4I_{11/2}$ transition was determined to be $\sigma_{{\rm abs}(n_x)} = 1.5 \times 10^{-20}$ cm^2, $\sigma_{{\rm abs}(n_y)} = 1.2 \times 10^{-20}$ cm^2, and $\sigma_{{\rm abs}(n_z)} = 2.0 \times 10^{-20}$ cm^2.

Measurements of the refractive indices of YCOB have also been presented by Mougel *et al.* [32]. The new single-pole Sellmeier equations to fit the indices were determined using the same relative orientation between the crystallographic axes and the optical indicatrices as described above. Our representation of the optical indicatrix axes is defined by adopting the traditional refractive-index convention $n_x < n_y < n_z$ [22]. For convenience, the Sellmeier equations are shown here for our convention [32]

$$n_X^2 = 2.7673 + \frac{0.020\,47}{\lambda^2 - 0.018\,63} - 0.006\,25\lambda^2 \qquad (2a)$$

$$n_Y^2 = 2.8730 + \frac{0.022\,59}{\lambda^2 - 0.017\,10} - 0.009\,21\lambda^2 \qquad (2b)$$

$$n_Z^2 = 2.9113 + \frac{0.022\,42}{\lambda^2 - 0.018\,73} - 0.012\,35\lambda^2 \qquad (2c)$$

where λ is the wavelength in micrometers. The measured and calculated line strengths of Nd^{3+} in YCOB are presented in Table I. An analysis by Mougel *et al.* [3], [33] on Nd^{3+} : GdCOB and Nd^{3+} : YCOB reported similar results.

The three Judd–Ofelt parameters $\Omega_t, t = 2, 4, 6$ shown in Table II are obtained by a least-squares fitting procedure. In performing the fitting routine, we have used the set of doubly reduced, unit-tensor operators for Nd^{3+} listed by Kaminskii [34]. The estimated rms error in determining the deviation in line strength is approximately 8%, as defined in [27]. A summation of the Ω_t parameters gives an effective Judd–Ofelt intensity parameter, which are presented in Table II.

The three Ω_t parameters determined from simple absorption measurements are then used to calculate the electric-dipole transition probability between any two J-manifolds [36]. The effective transition probabilities are then used to obtain the lifetime τ of an excited J-manifold [27]

$$\tau^{-1} = \sum_K A_{\rm eff}(J, K). \qquad (3)$$

The effective fluorescence branching ratio $\beta_{\rm eff}(J, K)$ from the manifold J to a lower lying manifold K is given by [27]

$$\beta_{\rm eff}(J, K) = A_{\rm eff}(J, K) \cdot \tau. \qquad (4)$$

The calculated lifetime and effective branching ratios from the ${}^4F_{3/2}$ manifold are given in Table II.

The emission cross section may be estimated with the Fuchtbauer–Landenburg formula [27]

$$\sigma_{\rm ems}(\lambda) = \frac{\lambda^2}{8\pi n^2 c} \cdot \frac{\beta_{\rm eff}(J, K)}{\tau} \cdot g(\nu) \qquad (5)$$

TABLE I
MEASURED AND CALCULATED LINE STRENGTHS OF ALL TRANSITIONS FROM THE $^4I_{9/2}J$ MANIFOLD TO THE J MANIFOLD INDICATED IN $Nd^{3+} : YCa_4O(BO_3)_3$

J-Manifold	$\bar{\lambda}$ (nm)	n_x E//X	S_{meas} (10^{-20} cm^2) E//X	n_x E//Y	S_{meas} (10^{-20} cm^2) E//Y	n_x E//Z	S_{meas} (10^{-20} cm^2) E//Z
$^4F_{3/2}$	880	1.670	0.194	1.702	0.544	1.712	1.35
$^4F_{5/2} + {}^2H_{9/2}$	812	1.672	1.54	1.704	1.04	1.714	3.56
$^4F_{7/2} + {}^4S_{3/2}$	742	1.674	1.47	1.706	0.71	1.717	2.4
$^4F_{9/2}$	675	1.677	0.13	1.709	0.057	1.720	0.355
$^4G_{5/2} + {}^2G_{7/2}$	590	1.681	4.06	1.714	2.38	1.725	4.22
$^4G_{9/2}$	515	1.688	0.97	1.721	0.715	1.732	1.9
$^2K_{15/2} + {}^2G_{9/2} + {}^2D_{3/2}$	470	1.693	0.184	1.727	0.215	1.738	0.589
$^2P_{1/2} + {}^2D_{5/2}$	430	1.700	0.048	1.734	0.149	1.745	0.37
$^2P_{3/2} + {}^2D_{3/2} + {}^4D_{3/2}$	355	1.720	1.06	1.755	1.5	1.766	3.15

TABLE II
EFFECTIVE JUDD–OFELT PARAMETERS AND EMISSION PARAMETERS OF $ND^{3+} : YCa_4O(BO_3)_3$

Effective Judd-Ofelt Parameters	Ω_2 (10^{-20} cm^2)	Ω_4 (10^{-20} cm^2)	Ω_6 (10^{-20} cm^2)	
	0.82	2.74	1.43	
Calculated Lifetime	680 μs			
Effective Branching Ratios ($^4F_{3/2}$)	$^4I_{9/2}$ (%)	$^4I_{11/2}$ (%)	$^4I_{13/2}$ (%)	$^4I_{15/2}$ (%)
	54	39.5	6.4	0.1

where λ is the wavelength and $g(\nu)$ is the normalized line-shape function [27]

$$g(\nu) = \frac{I(\nu)}{\int \frac{1}{3}[I_x(\nu) + I_y(\nu) + I_z(\nu)]\, d\nu}. \tag{6}$$

Calculation of the peak emission cross section $\sigma_p(J, K)$ from the normalized spectral emission is shown in Fig. 3 for the $^4F_{3/2} \rightarrow {}^4I_{9/2}$, $^4I_{11/2}$ and $^4I_{13/2}$ transitions.

The radiative fluorescence lifetime of the excited $^4F_{3/2}J$ manifold in Nd^{3+} : YCOB at room temperature was measured for three concentrations (2%, 5%, and 10%) of Nd_2O_3 placed in the melt. Using both powder and optically thin polished samples, the fluorescence lifetime was measured using a birefringently tuned Q-switched Cr : $LiSrAlF_6$ laser. The laser was used to excite the samples at 812 nm. The Nd^{3+} lifetime varied from 102 to 95 μs with a single exponential decay. The small change in fluorescence lifetime suggests very little concentration quenching at these low dopant concentrations. Comparing the measured radiative lifetime to the calculated lifetime using the Judd–Ofelt parameters implies a low quantum efficiency of 15% for the Nd : YCOB laser. This low efficiency has been explained as a multiphonon nonradiative relaxation process [3].

IV. LASER PERFORMANCE

A number of techniques have been devised to scale the overall pump power of end-pumped solid-state lasers. These include the use of polarization combination, high-power diode bars, multiple sources using fiber bundles [36], [37], or multiple entrances to many gain elements [38]. We demonstrate here a novel technique for combining in free space the light from four separate multimode laser diodes for improved pump-power density. Angular-multiplexing individual high-brightness laser diodes was first described by Fan *et al.* [39], [40]. They used three diode lasers closely packed in the plane perpendicular to the junction and a combination of cylindrical lenses to collimate and focus the light [39]. The high-brightness multilaser source, developed by the Polaroid Corporation [41], similarly places the near-field images of up to eight separate multimode diode lasers side-by-side on a multifaceted mirror, which redirects the beams so they are juxtaposed and parallel [41]. The diode-laser packages (illuminators) are arranged roughly on a circle with the plane parallel to the junction placed perpendicular to the optical axis. Each illuminator consists of a 100-μm strip-width diode laser, a microlens, and anamorphic optics. The mirror is monolithic with eight diamond-turned facets, each having a projected width in the output direction of 300 μm, giving a full projected width of 2.4 mm [41].

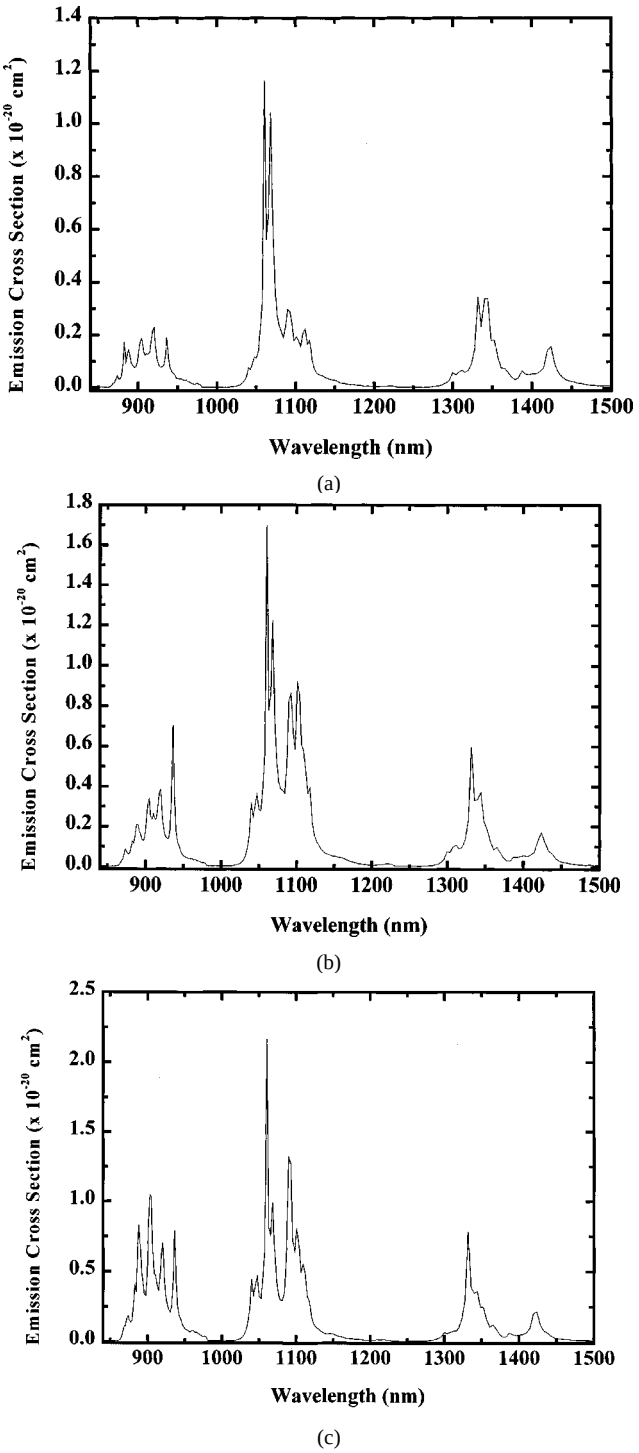

Fig. 3. Emission spectra for light polarized along the (a) X, (b) Y, and (c) Z optical indicatrix axes of $Nd^{3+}:YCa_4O(BO_3)_3$.

Two advantages, relative to diode bars, of using individual high-brightness laser diodes are the individual controls over their wavelength and their polarization. Separate temperature control for each laser diode allows one to generate an overall spectral output that is tightly matched to a narrow absorption peak (<0.8-nm FWHM). In addition, the overall output from the high-brightness source can be linearly polarized.

Additional optics were placed on the output of the multidiode high-brightness source to reduce the output spot-size and

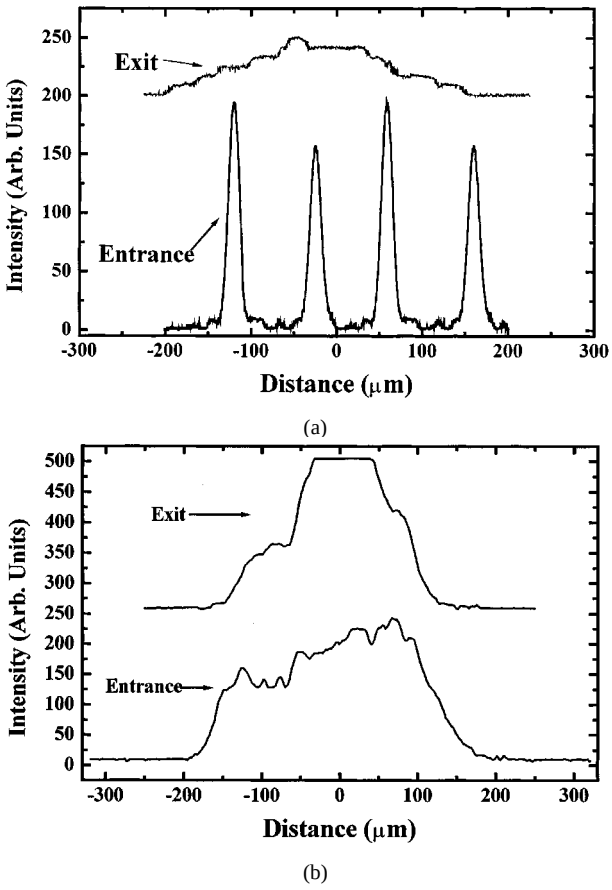

Fig. 4. Intensity profiles of the pump beam along the propagation direction. In both cases, the bottom trace is the nearest to the pump source (entrance) and the top trace is the farthest (exit). (a) The plane perpendicular to the junction. (b) The plane parallel to the junction.

focus the light into the crystal. The output from four diode lasers generated an overall beam size of ~700 by 900 μm. A 2 : 1 reducing spherical telescope (100 mm plano/concave and 50 mm plano/convex) was then used to produce a rectangular beam of ~375 by 405 μm. This light was then focused using a spherical 50-cm focal-length lens to pump mode spot-sizes of 290×300 μm (FWHM). Fig. 4 shows the typical pump-beam profile near the focus in the planes perpendicular and parallel to the junction. The profiles were measured with a scanning-slit beam-profiler (Photon Inc.) The four laser-beams were not found to be completely parallel. This effect was also seen in attempts with larger-ratio beam-reducers, which resulted in larger pump-mode spot-sizes because the individual beams were diverging from each other. The principal loss in brightness occurs because the mirror facets are 300 μm wide and the near-field images formed on them are only 50 μm, giving an inherent 6 : 1 loss [41]. Smaller facets and tighter tolerances on the alignment to increase parallelism would increase the brightness of the source.

The laser resonator consisted of a flat pump input mirror M_1 and a concave output mirror M_2. The pump-laser polarization was parallel to the Z axis and focused into the crystal through the rear mirror, which was 96% transparent at 812 nm. The reflectivity of M_1 was $R > 99.9\%$ for both the fundamental and the second-harmonic wavelengths. Three different output-coupling mirrors, M_2, were used for operating the laser

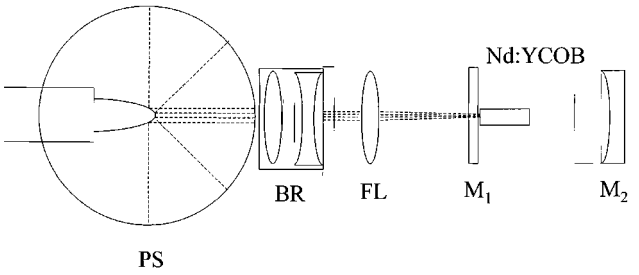

Fig. 5. Schematic of the end-pumped SFD $Nd^{3+}:YCa_4O(BO_3)_3$ laser system.

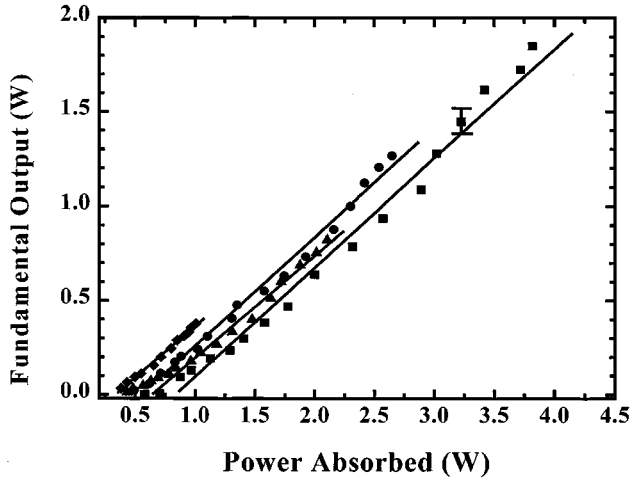

Fig. 6. Fundamental laser output at 1060 nm using a 2% output coupler. Pumping is by one (♦), two (▲), three (●), or four (■) laser diodes.

in either the fundamental or SFD modes of operation. The mirrors used were highly reflecting or had an output coupling of 1% or 2% at 1060 nm with a 10-cm radius of curvature. The highly reflecting mirror was also coated to be highly transmissive at 530 nm ($T > 94\%$). The laser cavity was near hemispherical and was operated close to the limit of optical stability. The laser crystal was mounted between two copper blocks. Each block was temperature controlled using thermoelectric coolers, which were heat-sunk to two water-cooled aluminum blocks. The laser-crystal holder was secured to a two-axis rotational-adjustment kinematic mount.

The $Nd^{3+}:YCOB$ crystal was pumped with up to four diode lasers using the multilaser high-brightness source. A schematic of the end-pumped SFD $Nd^{3+}:YCOB$ laser is shown in Fig. 5. The surfaces of the pump optics were not AR-coated for the pump wavelength. Thus, the transmission of the pump optics was only 90% at 812 nm. The focus of the pump beam was located on the front facet of the $Nd^{3+}:YCOB$ crystal, which was placed next to the flat high reflector.

Fundamental laser operation is shown in Fig. 6. The CW laser output was characterized using up to four diode laser pump sources. A laser slope efficiency of 55%–57% was achieved in each case with the absorbed pump-power threshold ranging from 380 to 520 mW. This result indicates that not all the diode lasers were pumping the same cavity mode volume [39]. The increase in threshold with increasing number of diode lasers indicates an increase in the pump mode volume, which reduces pump beam brightness.

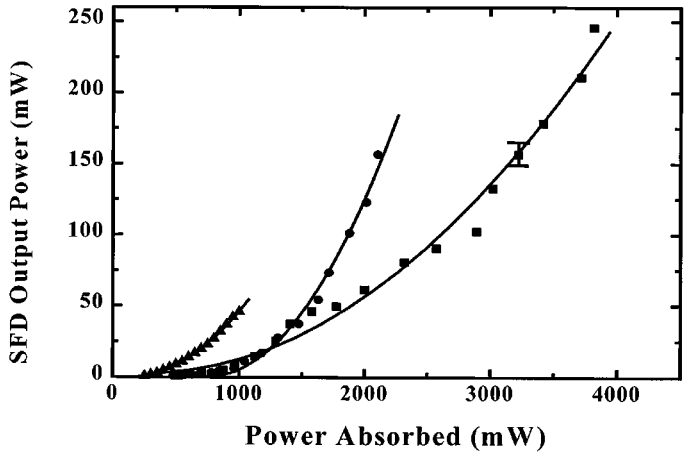

Fig. 7. Self-frequency-doubled laser output at 530 nm. Pumping is by one (♦), two (▲), or four (■) laser diodes.

Scaling of SFD by increasing the number of diode lasers was also investigated. Fig. 7 shows SFD laser operation of $Nd^{3+}:YCOB$ for 1, 2, and 4 diode-laser pump sources. At the maximum pump power of 3.8 W, the laser generated more than 245 mW of visible 530-nm radiation. To our knowledge, this is the highest output power in the visible region using a diode-pumped SFD laser. With a total pump power of 6.9 W from the four laser diodes, a conversion efficiency of 3.6% was obtained. The highest conversion efficiency of 4.6% was obtained using only two laser diodes. From Fig. 4, we see the best pump mode was obtained for the described cavity (cavity waist $\sim$85 μm). Likewise, the operation with a single diode produced a conversion efficiency of only 2.3%. By inspecting the conversion efficiencies for all three cases presented, we see that efficient extraction of the pump mode into the laser mode volume is equally important as obtaining a small cavity waist. By increasing the size of the cavity waist, improved laser operation should be obtained. However, it should be noted that this would reduce the intracavity power density, which would in turn decrease the nonlinear coupling of the fundamental to the second-harmonic wave. This has been previously demonstrated [12], and, thus, a compromise is made to obtain optimum SFD operation. From our own inspection of Fig. 7, we see that two diode lasers produce an optimum conversion of pump light to second-harmonic light. A reduction in efficiency with four diode lasers corresponds to less mode overlap for fundamental operation, reducing the second-harmonic conversion process. Additional effects such as thermal lensing and temperature variations of the phase-matching condition may also be effecting the efficiency at these high pump power levels.

The beam-quality parameters for the SHG and fundamental operation were measured with a scanning slit beam-profiler. The beam-quality measurement was obtained by generating a beam waist using a lens [42]. For the second harmonic, $M^2 = 6.2$ and 5.3 for the parallel and perpendicular planes to the optical axis. The fundamental laser output had a beam-quality measurement of $M^2 = 3.6$ and 1.9 for the parallel and perpendicular planes to the optical axis, respectively.

As with most intracavity frequency-doubled lasers with many oscillating longitudinal modes, the SFD process in

Nd^{3+} : YCOB has a large amplitude fluctuation due to longitudinal mode coupling through the sum-frequency generation process, which strongly modulates the second-harmonic light [43]. This noise can be shown either as a typical oscilloscope trace in time or as a noise percentage integrated over bandwidth. A measure of the highest power spike and lowest power spike can give large deviations in the peak-to-peak noise level. Here, we have measured the amplitude stability in terms of the spectral density of the relative intensity noise (RIN) [44], [45]. The RIN was measured by detecting the 530-nm light using a silicon photodiode and passing this signal to a spectrum analyzer. The relationship between RIN when expressed in dB/Hertz and the rms noise is [45]

$$\text{rms} = \sqrt{\int_{f_{\min}}^{f_{\max}} \text{RIN}(f)\, df} \tag{7}$$

where $f_{\min}$ and $f_{\max}$ determine the range of the rms noise bandwidth. Here, we have determined the rms noise to be 3.1% for the case of maximum green emission. This is worse than the previously published measurement of 8% peak-to-peak noise fluctuation since in practice the peak-to-peak noise is four times the rms noise [45]. Other SFD lasers have had between 3% and 6% peak-to-peak amplitude fluctuation [46]. This rms noise fluctuation is a consequence of not only multilongitudinal mode oscillations but also coupled polarization modes [47] and feedback instabilities on the laser diode source due to the absence of AR coatings on the pump optics. There are several methods of suppressing the chaotic instabilities and noise associated with green lasers [48]–[50]. However, in these experiments, no attempts were made to reduce the rms noise of the SFD output. Future cavity designs will include measures to limiting amplitude fluctuations.

V. Material Properties and Thermal Fracture Limits

The optical pumping process of all-solid-state lasers generates some amount of localized heating of the laser material. Heating results from several causes: quantum defect, quenching mechanisms, thermalized terminal laser level(s), and absorption of the pump photons by the host material [51]. In the limit, the combination of volumetric heating and surface cooling can result in thermo-mechanical failure from stress.

Stress fracture occurs when the stress induced by temperature gradients in the laser material exceeds the tensile strength of the material. The mechanical properties of the laser host material determine the maximum surface stress that can be tolerated prior to fracture. The thermal loading and thus average output power of a laser in a rod or slab could be increased until stress fracture occurred. The maximum absorbed thermal power per unit length by a laser rod for slab geometry is [52], [53]

$$\frac{Pa}{l} = 12 \cdot R_T \cdot \frac{w}{t} \tag{8}$$

where w/t is the aspect ratio of width to thickness and R_T is a thermal stress resistance figure of merit (FOM) for the material. The FOM is valid for a given flaw size and is dependent on the intrinsic material properties [51], [53].

TABLE III
Thermal Loading and Estimated Thermal-Fracture FOM for Nd^{3+} : $YCa_4O(BO_3)_3$

	230 μm	620 μm	930 μm
P_a/L (W/m)	3410	2950	2520
R_t (W/m)	280	250	210

In some experiments of thermal stress fracture, we measured the power absorbed per unit length to determine the value R_T. We began by measuring the power incident on the crystal. Using the well-known Beer's law [51], we calculated the power absorbed over the length of the crystal up to the point where subsurface cracking occurred.

In three experiments, the initial input power on the front face of the crystal was measured to be 13.5, 12.3 and 10.9 W with the associated fracture occurring at 0.23, 0.62, and 0.93 mm beyond the input face, respectively. Although these measurements are fracture-size-dependent, all three propagated cracks ranged from 50 to 100 μm in width. Table III gives the associated power absorbed per unit length and a calculated thermal stress-resistance FOM. The estimated FOM is better than that of $YLiF_4$ and is comparable to silicate glass [27]. However, using the measured thermal conductivity and thermal expansion values with reasonably estimated values for elastic modulus, Poisson's ratio, and tensile fracture strength, we see the thermal stress FOM to be 1.5 to 2 times the experimentally determined values. Given the difficult nature of such a measurement, we believe the values given in Table III to be reasonable first-order estimates.

VI. Conclusions

In this paper, we have investigated scaling of a diode-pumped SFD laser crystal, Nd^{3+} : YCOB, to higher output powers at visible wavelengths. We have performed spectroscopic measurements to determine the absorption coefficient and emission cross section of the material. Scaling of SFD laser action to the fracture limit of the crystal, using an innovative pump-source, having multiple high-brightness laser-diodes, has been demonstrated. The highest output SFD power of 245 mW at 530 nm was achieved. The material fracture limits were also determined experimentally and compared to calculated results. Like all end-pumped lasers, the brightness of the pump-source diode(s) and, ultimately, the fracture limits of the laser host material, limit the peak power. With SFD lasers, the brightness of the pump has a more direct impact on the SHG conversion efficiency than with traditional intracavity-doubling techniques, which can compensate for larger, circulating cavity modes.

Acknowledgment

The authors would like to thank the software and electronic support by S. Wang of B&W TEK for the pump source power supply. They also acknowledge the invaluable technical support of N. Vanasse for the thermo/mechanical mounting systems and useful discussion with J. Eichenholz.

REFERENCES

[1] S. Nakamura, "InGaN/GaN/AlGaN-based laser diodes with cleaved facets grown on GaN substrates," *Appl. Phys. Lett.*, vol. 73, pp. 832–834, 1998.

[2] B. H. T. Chai, "Advances in bulk inorganic nonlinear optical materials," *Opt. Photon. News*, vol. 10, pp. 31–38, 1999.

[3] F. Mougel, G. Aka, A. Kahn-Harari, H. Hubert, J. M. Benitez, and D. Vivien, "Infrared laser performance and self-frequency doubling of $Nd^{3+}:Ca_4GdO(BO_3)_3$ (Nd : GdCOB)," *Opt. Mater.*, vol. 8, pp. 161–173, 1997.

[4] J. M. Eichenholz, D. A. Hammons, L. Shah, Q. Ye, R. E. Peale, M. Richardson, and B. H. T. Chai, "Diode-pumped self-frequency doubling in $Nd^{3+}:YCa_4O(BO_3)_3$ laser," *Appl. Phys Lett.*, vol. 74, pp. 1954–1956, 1999.

[5] F. Mougel, F. Augé, G. Aka, A. Kahn-Harari, D. Vivien, F. Balembois, P. Georges, and A. Brun, "New green self-frequency doubling diode-pumped Nd:$Ca_4GdO(BO_3)_3$ laser," *Appl. Phys. B*, vol. 67, pp. 533–535, 1998.

[6] Q. Ye, L. Shah, J. Eichenholz, D. Hammons, R. Peale, M. Richardson, A. Chin, and B. H. T. Chai, "Investigation of diode-pumped, self-frequency doubled RGB lasers from Nd : YCOB crystals," *Opt. Commun.*, vol. 164, pp. 33–37, 1999.

[7] D. A. Hammons, J. M. Eichenholz, Q. Ye, B. H. T. Chai, L. Shah, R. E. Peale, M. Richardson, and H. Qiu, "Laser action in $Yb^{3+}:YCOB$ ($Yb^{3+}:YCa_4O(BO_3)_3$)," *Opt. Commun.*, vol. 156, pp. 327–330, 1998.

[8] F. Mougel, K. Dardenne, G. Aka, A. Kahn-Harari, and D. Vivien, "Yterbium-doped $Ca_4GdO(BO_3)_3$: an efficient infrared laser and self-frequency doubling crystal," *J. Opt. Soc. Amer. B*, vol. 16, pp. 164–172, 1999.

[9] L. F. Johnson and A. A. Ballman, "Coherent emission from rare earth ions in electro-optic crystals," *J. Appl. Phys.*, vol. 40, pp. 297–302, 1969.

[10] V. G. Dmitriev, E. V. Raevskii, N. M. Rubina, L. N. Rashkovich, O. O. Silichev, and A. A. Romichev, "Simultaneous emission at the fundamental frequency and the second harmonic in an active nonlinear medium: neodymium-doped lithium metaniobate," *Sov. Tech. Phys. Lett.*, vol. 5, pp. 590–591, 1979.

[11] A. Cordova-Plaza, T. Y. Fan, M. J. F. Digonnet, R. L. Byer, and H. J. Shaw, "$Nd:MgO:LiNbO_3$ continuous-wave laser pumped by a laser diode," *Opt. Lett.*, vol. 13, pp. 209–211, 1988.

[12] J. Bartschke, R. Knappe, K.-J. Boller, and R. Wallenstein, "Investigation of efficient self-frequency-doubling Nd : YAB lasers," *IEEE J. Quantum Electron.*, vol. 33, pp. 2295–2300, 1997.

[13] D. Jaque, J. Capmany, J. García Solé, Z. D. Luo, and A. D. Jiang, "Continuous—Wave laser properties of the self-frequency-doubling $YAl_3(BO_3)_4$: Nd crystal," *J. Opt. Soc. Am. B*, vol. 15, pp. 1656–1662, 1998.

[14] B. Lu, J. Wang, H. Pan, and M. Jiang, "Laser self-doubling in neodymium yttrium aluminum borate," *J. Appl. Phys.*, vol. 66, pp. 6052–6058, 1989.

[15] D. Jaque, J. Capmany, and J. García Solé, "Continuous wave laser radiation at 669 nm from a self-frequency-doubled laser of $YAl_3(BO_3)_4:Nd^{3+}$," *Appl. Phys. Lett.*, vol. 74, pp. 1788–1790, 1999.

[16] J. Capmany, D. Jaque, J. García Solé, and A. A. Kaminskii, "Continuous-wave laser laser radiation at 524 nm from a self-frequency-doubled laser of $LaBGeO_5:Nd^{3+}$," *Appl. Phys. Lett.*, vol. 72, pp. 531–533, 1998.

[17] A. A. Kaminskii, "Ferroelectric $Nd^{3+}:Sr_XBa_{1-X}(NbO_3)_3$—A new nonlinear laser crystal cw 1-micrometer stimulated emission ($^4F_{3/2} \rightarrow {}^4I_{11/2}$) and diffuse self-frequency double," *Quantum Electron.*, vol. 28, pp. 1031–1033, 1998.

[18] P. Wang, J. M. Dawes, P. Dekker, D. S. Knowles, J. A. Piper, and B. Lu, "Growth and evaluation of ytterbium-doped yttrium aluminum borate as a potential self-doubling laser crystal," *J. Opt. Soc. Amer. B*, vol. 16, pp. 63–68, 1999.

[19] E. Montoya, J. Capmany, L. E. Bausá, T. Kellner, A. Diening, and G. Huber, "Infrared and self-frequency doubled laser action in Yb^{3+}-doped $LiNbO_3:MgO$," *Appl. Phys. Lett.*, vol. 74, pp. 3113–3115, 1999.

[20] Q. Ye and B. H. T. Chai, "Crystal growth of $YCa_4O(BO_3)_3$ and its orientation," *J. Cryst. Growth*, vol. 197, pp. 228–235, 1999.

[21] M. Iwai, T. Kobayashi, H. Furuya, Y. Mori, and T. Sasaki, "Crystal growth and optical characterization of rare-earth (Re) calcium oxyborate $ReCa_4O(BO_3)_3$ (Re = Y or Gd) as a new nonlinear optical material," *Jpn. J. Appl. Phys.*, vol. 36, pp. L276–L279, 1997.

[22] *Handbook of Nonlinear Optical Crystals*, 2nd ed., Springer-Verlag, Berlin, Germany, 1996.

[23] R. Norrestam, M. Nygren, and J. O. Bovin, "Structural investigations of new calcium—Rare earth (R) oxyborates with the composition $Ca_4RO(BO_3)_3$," *Chem. Mater.*, vol. 4, pp. 737–743, 1992.

[24] TBAR coating, Quality Thin Films Inc., Oldsmar, FL.

[25] Q. Ye, "Investigation of self-frequency doubling crystals, $YCa_4O(BO_3)_3$, (YCOB), doped with neodymium or ytterbium," Ph. D. dissertation, Univ. of Central Florida, Orlando, FL, 1999.

[26] B. Henderson and G. F. Imbusch, *Optical Spectroscopy of Inorganic Solids*. New York, NY: Oxford Univ. Press, 1989, pp. 274–278.

[27] W. F. Krupke, M. D. Shinn, J. E. Marion, J. A. Caird, and S. E. Stokowski, "Spectroscopic, optical, and thermomechanical properties of neodymium- and chromium–doped gadolinium scandium gallium garnet," *J. Opt. Soc. Amer. B*, vol. 3, pp. 102–113, 1986.

[28] A. J. Alfrey, O. M. Stafsudd, B. Dunn, and D. L. Yang, "Analysis of the absorption spectrum of neodymium : sodium beta double prime alumina," *J. Chem. Phys.*, vol. 88, pp. 707–716, 1987.

[29] H. Dai and O. M. Stafsudd, "Polarized absorption spectrum and intensity analysis of trivalent neodymium in sodium β'' Alumina," *J. Phys. Chem. Solids*, vol. 52, pp. 367–379, 1991.

[30] J. R. Ryan and R. Beach, "Optical absorption and stimulated emission of neodymium in yttrium lithium fluoride," *J. Opt. Soc. Amer. B*, vol. 9, pp. 1883–1887, 1992.

[31] T. S. Lomheim and L. G. DeShazer, "Optical absorption and fluorescence intensities of Nd^{3+} in garnets $CaY_2Mg_2Ge_3O_{12}$ and $Gd_3Ga_5O_{12}$ and the biaxial crystal $La_2Be_2O_5$," *Phys. Rev. B*, vol. 20, pp. 4343–4356, 1979.

[32] F. Mougel, G. Aka, F. Salin, D. Pelenc, B. Ferrand, A. Kahn-Harari, and D. Vivien, "Accurate second harmonic generation phase matching angles prediction and evaluation of non linear coefficients of $Ca_4YO(BO_3)_3$ (YCOB) crystal," *Advanced Solid-State Lasers—OSA Trends in Opt. Photon. Ser.*, vol. 26, pp. 709–714, 1999.

[33] F. Mougel, G. Aka, J. M. Benitez, A. Kahn-harari, and D. Vivien, "Spectroscopic investigations of the $^4F_{3/2} \rightarrow {}^4I_{9/2}$ neodymium channel of Nd : GdCOB and Nd : YCOB for infrared and blue laser emission," *Advanced Solid-State Lasers—OSA Trends in Opt. Photon. Ser.*, vol. 26, pp. 625–630, 1999.

[34] A. A. Kaminskii, *Crystalline Lasers: Physical Processes and Operating Schemes*. Boca Raton, FL: CRC Press, 1996.

[35] W. F. Krupke, "Induced-emission cross sections in neodymium laser glasses," *IEEE J. Quantum Electron.*, vol. QE-10, pp. 450–457, 1974.

[36] K. Kubodera and J. Noda, "Pure single-mode $LiNdP_4O_{12}$ solid-state laser transmitter for 1.3-μm fiber-optic communications," *Appl. Opt.*, vol. 21, pp. 3466–3469, 1982.

[37] J. Berger, D. F. Welch, W. Streifer, D. R. Scifres, N. J. Hoffman, J. J. Smith, and D. Radecki, "Fiber-bundle coupled, diode end-pumped Nd : YAG laser," *Opt. Lett.*, vol. 13, pp. 306–308, 1988.

[38] J. Frauchiger, P. Albers, and H. P. Weber, *Dig. Topical Meet. Tunable Solid-State Lasers*, 1989, TuC2.

[39] T. Y. Fan, A. Sanchez, and W. E. DeFeo, "Scalable, end-pumped, diode-laser-pumped laser," *Opt. Lett.*, vol. 14, pp. 1057–1059, 1989.

[40] C. P. Wyss, W. Lüthy, H. P. Weber, L. Brovelli, C. Harder, and H. P. Meier, "A diode-laser pump source with small focus diameter for end-pumped systems," *Opt. Quantum Electron.*, vol. 31, pp. 173–181, 1999.

[41] D. S. Goodman, W. L. Gordon, R. Jollay, J. W. Roblee, P. Gavrilovic, D. Kuksenkov, A. Goyal, and Q. Zu, "High brightness multi-laser source," *Proc. SPIE*, vol. 3626A, pp. 1–14, 1999.

[42] D. Wright, P. Greve, J. Fleischer, and L. Austin, "Laser beam width, divergence and beam propagation factor—An international standardization approach," *Opt. Quantum Electron.*, vol. 24, pp. S993–S1000, 1992.

[43] T. Baer, "Large-amplitude fluctuations due to longitudinal mode coupling in diode-pumped intracavity-doubled Nd : YAG lasers," *J. Opt. Soc. Amer. B*, vol. 3, pp. 1175–1180, 1986.

[44] T. J. Kane, "Intensity noise in diode-pumped single-frequency Nd : YAG Lasers and its control by electronic feedback," *IEEE Photon. Technol. Lett.*, vol. 2, pp. 244–245, 1990.

[45] ——, "Laser diode-pumped solid-state lasers," in *Conf. Laser Electro. Opt.*, 1997, pp. VI10–VI11.

[46] H. Hemmati, "Diode-pumped self-frequency-doubled neodymium yttrium aluminum borate (NYAB) laser," *IEEE J. Quantum Electron.*, vol. 28, pp. 1169–1171, 1992.

[47] M. Oka and S. Kubota, "Stable intracavity doubling of orthogonal linearly polarized modes in diode-pumped Nd : YAG lasers," *Opt. Lett.*, vol. 13, pp. 805–807, 1988.

[48] J. L. Nightingale and J. K. Johnson, "Single frequency ring laser with two reflecting surfaces," U.S. Patent 5 052 815, 1992.

[49] W. L. Nighan, J. Cole, and T. M. Baer, "Diode pumped, multi axial mode, intracavity doubled laser," U.S. Patent 5 446 749, 1995.

[50] L. R. Marshall, "Passively stablized intracavity doubling laser," U.S. Patent 5 511 085, 1996.
[51] W. Koechner, *Solid-State Laser Engineering*, 3rd ed. Berlin, Germany: Springer-Verlag, 1992.
[52] J. M. Eggleston, T. J. Kane, K. Kuhn, J. Unternahrer, and R. L. Byer, "The slab geometry laser—Part 1: Theory," *IEEE J. Quantum Electron.*, vol. QE-20, pp. 289–301, 1984.
[53] D. S. Sumida and B. A. Wechsler, "Laser host crystals: physical, optical, and thermomechanical properties," in *Conf. Laser Electro. Opt.*, 1997.

Dennis A. Hammons, photograph and biography not available at the time of publication.

Martin Richardson, photograph and biography not available at the time of publication.

Bruce H. T. Chai, photograph and biography not available at the time of publication.

A. K. Chin, photograph and biography not available at the time of publication.

R. Jollay, photograph and biography not available at the time of publication.